Effects of electron–acoustic phonon interaction in the presence of spin–orbit couplings in graphene

ARTICLE *in* PHYSICA B CONDENSED MATTER · SEPTEMBER 2015

Impact Factor: 1.32 · DOI: 10.1016/j.physb.2015.05.029

1 AUTHOR:

Aybey Mogulkoc

Radboud University Nijmegen

13 PUBLICATIONS **26** CITATIONS

SEE PROFILE

Physica B 473 (2015) 20–25

Contents lists available at ScienceDirect

Physica B

journal homepage: www.elsevier.com/locate/physb

Effects of electron–acoustic phonon interaction in the presence of spin–orbit couplings in graphene

A. Mogulkoc

Department of Physics, Faculty of Sciences, Ankara University, 06100 Tandoğan, Ankara, Turkey

ARTICLE INFO

Article history:
Received 25 November 2014
Received in revised form
3 May 2015
Accepted 23 May 2015

Keywords:
Graphene
Electron–phonon interaction
Spin–orbit coupling

ABSTRACT

We investigate the effects of electron-zone center acoustic phonon interaction on spin–orbit couplings in pristine graphene. We examine the polaron formation and analyse the effects of spin–orbit couplings on polaron formation and electron–phonon couplings. Fröhlich type Hamiltonian within the continuum limit is used to describe the electron–phonon system. With theoretical analysis, we show that, in the presence of electron–phonon interaction, the intrinsic and Rashba spin–orbit couplings of graphene become k dependent and Rashba spin–orbit coupling exhibits different characters with respect to spin orientation. Even there is a symmetry between electron–hole states if only one spin–orbit mechanism is present, electron–phonon coupling induces symmetry breaking between electron–hole states. Moreover, polaronic effect is decreased for both spin states, but it is increased beyond the some critical values of k for spin-up states in the presence of spin–orbit couplings.

1. Introduction

Since the synthesis of graphene [1,2], due to its fascinating physical properties, graphene have become one of the hot topics of current research in condensed matter physics. Spin–orbit interaction mechanism is crucial for graphene physics, because of its applications in spintronics. The manipulation of the spin of electrons may enable spin-based nanoscale devices generated from this promising material. The effects of intrinsic and Rashba spin–orbit couplings in the graphene were first examined by Kane and Mele in this conjecture [3,4]. The intrinsic spin–orbit coupling (ISOC) in pristine graphene is very weak, about $\Delta = 0.01$–0.05 meV [5,6], it can be neglected in many cases. The origin of Rashba spin–orbit coupling (RSOC) is thought as a consequence of the external electrical field or the substrate. Recent experiments have shown that the giant RSOC of the π bands in graphene when deposited on Ni (111) is found to be around $\lambda = 225$ meV [7], and also Au intercalation at the graphene–Ni interface yields another giant RSOC, i.e., order of $\lambda = 100$ meV [8]. Giant RSOC of graphene may be used in potential spintronic devices, i.e., Das-Datta spin field-effect transistor [9,10], due to the symmetry breaking between up and down spin states. In the literature, there are also some recent works on spin–orbit couplings of graphene that investigate the effects on the other physical properties of graphene and graphene based nano-structures [6,8,11–24]. It is also well-known that the phonon modes of graphene play an important role in charge carriers dynamics. It was shown that interaction of charge carriers with zone center doubly degenerate optical phonons yield polaron formation, and reduce the Fermi velocity [25,26]. Charge carriers can also interact with acoustic phonon modes as well as the optical phonon modes. Since the electron and acoustic phonons with having alinear dispersion couple by a short range potential, it is believed that this coupling plays an important role for formation of self-trapped state [27]. Self-trapping mechanism of acoustic polarons has been examined in some studies [28–31]. Moreover, effects of electron–phonon interaction in low-dimensional structure with spin–orbit couplings is another crucial issue that enables the manipulation of spin states giving rise to inspiration for spintronic devices. In the presence of both interaction, physical properties of two-dimensional electron gas, semiconductor heterostructures, and graphene have been examined in some previous works [32–39]. While most of these works [32–36] claimed that the polaronic effect has enhanced with spin–orbit coupling mechanisms in conventional two-dimensional systems, Covaci and Berciu showed that the RSOC decreases the effective electron–phonon coupling and leads to different conductivities for the two spin polarizations [37]. In an another work, in the presence of electron–LO–phonon interaction with two spin–orbit couplings (Rashba and Dresselhaus) yield anisotropy in the self-energy correction of graphene electron energy, and they lead to either weaker or stronger polaronic effect with respect to the direction [38].

E-mail address: mogulkoc@science.ankara.edu.tr

http://dx.doi.org/10.1016/j.physb.2015.05.029
0921-4526/

In this paper, we investigate the interaction of graphene charge carriers with zone center acoustic phonons in the presence of spin–orbit couplings, and we examine the variation of spin–orbit couplings due to the electron–phonon coupling. We follow an analytical method based on Lee–Low–Pines (LLP) theory [40]. Firstly, we find the eigenvalues and eigenfunctions of two-sublattice system with real spin through the consideration of spin–orbit couplings. Secondly, we consider electron–phonon interaction Hamiltonian together with phonon subsystem, as well as spin–orbit couplings. We perform two successive unitary transformation to diagonalize the whole Hamiltonian. Finally, we analyse the associated polaronic effect related with both RSOC and ISOC. To the best our knowledge, this study is the first theoretical treatment considering the bilateral variation of electron–phonon and spin–orbit couplings of graphene.

2. Theory

In the continuum model, the interaction Hamiltonian of the graphene that includes SOC and electron–acoustic phonon couplings in the vicinity of K point can be written as

$$\mathcal{H} = \mathcal{H}_0 + \mathcal{H}_{\mathrm{SOC}} + \sum_{\boldsymbol{q},\mu} \hbar\omega_\mu(\boldsymbol{q}) b^\dagger_{\mu,\boldsymbol{q}} b_{\mu,\boldsymbol{q}} + \mathcal{H}_{\mathrm{e-p}} \tag{1}$$

where $\mathcal{H}_0 = \mathbf{1} \otimes v_F \boldsymbol{\sigma}\cdot\boldsymbol{p}$ is the unperturbed part, and

$$\mathcal{H}_{\mathrm{SOC}} = \frac{\lambda}{2}(s_y \otimes \sigma_x - s_x \otimes \sigma_y) + \Delta s_z \otimes \sigma_z \tag{2}$$

is the spin–orbit interaction Hamiltonian. Here, λ is the RSOC constant, Δ is the ISOC constant, and μ represents the branch of the zone center acoustic phonon. In Eq. (2), both $\boldsymbol{\sigma}$ and $\boldsymbol{s}$ are well-known Pauli spin matrices that represent real spin and pseudospin. In the absence of the electron–phonon interaction and bare phonon Hamiltonian, the corresponding eigenfunctions and eigenvalues of Eq. (1) can easily be constructed:

$$\langle \boldsymbol{r}|ts\boldsymbol{k}\rangle = \frac{1}{\sqrt{2}L}\frac{\exp(i\boldsymbol{k}\cdot\boldsymbol{r})(\hbar v_F k)}{\left(\sqrt{(\hbar v_F k)^2 + (E_{ts} - \Delta)^2}\right)}\begin{pmatrix} -sie^{-i2\theta(\boldsymbol{k})} \\ \dfrac{-sie^{-i\theta(\boldsymbol{k})}}{(\hbar v_F k)}(E^{ts}_{\mathrm{SOC}} - \Delta) \\ \dfrac{e^{-i\theta(\boldsymbol{k})}}{(\hbar v_F k)}(E^{ts}_{\mathrm{SOC}} - \Delta) \\ 1 \end{pmatrix}, \tag{3}$$

and

$$E^{ts}_{\mathrm{SOC}} = s\frac{\lambda}{2} + t\sqrt{(\hbar v_F k)^2 + \left(\frac{\lambda}{2} - s\Delta\right)^2} \tag{4}$$

where L^2 is the total area of the system, $v_F \cong 10^6$ is the Fermi velocity, s and t are the spin and pseudospin index, respectively. While s takes + (↑ spin) and − (↓ spin) values, t takes + (A sublattice) and − (B sublattice) values. In Eq. (1), the last term represents the electron–phonon couplings [41], and is given by

$$\mathcal{H}_{\mathrm{e-p}} = \mathbf{1} \otimes \frac{3\beta\gamma}{a^2}\begin{pmatrix} 0 & u_{xx}(\boldsymbol{r}) - u_{yy}(\boldsymbol{r}) + 2iu_{xy}(\boldsymbol{r}) \\ u_{xx}(\boldsymbol{r}) - u_{yy}(\boldsymbol{r}) - 2iu_{xy}(\boldsymbol{r}) & 0 \end{pmatrix} \tag{5}$$

where $\beta = -\,d\ln J_0/d\ln a$, $\gamma = \left(3a/2\right)J_0$, J_0 is the resonance integral between nearest neighbor carbon atoms which is of order of 2.77 eV, a is the carbon–carbon inter-distance bond length, i.e., 1.42 Å^{-1}. In Eq. (5), the matrix elements can be defined as

$$u_{xx} = (\partial u_x/\partial x), \quad u_{yy} = (\partial u_y/\partial y), \quad 2u_{xy} = (\partial u_x/\partial x)(\partial u_y/\partial y)$$
$$u_\mu(\boldsymbol{r}) = \sum_{\boldsymbol{q}} \sqrt{\frac{\hbar}{2NM_C\omega_\mu(\boldsymbol{q})}}(b_{\boldsymbol{q},\mu} + b^\dagger_{\boldsymbol{q},\mu})\varepsilon_\mu(\boldsymbol{q})e^{i\boldsymbol{q}\cdot\boldsymbol{r}} \tag{6}$$

with polarization vectors

$$\varepsilon_{LA}(\boldsymbol{q}) = \frac{i}{|\boldsymbol{q}|}(q_x, q_y), \quad \varepsilon_{TA}(\boldsymbol{q}) = \frac{i}{|\boldsymbol{q}|}(-q_y, q_x)$$

where N is the number of unit cells, M_C is the mass of a carbon atom. In Eq. (4), $b_{\boldsymbol{q},\mu}$ and $b^\dagger_{\boldsymbol{q},\mu}$ are, respectively, the phonon annihilation and creation operators with phonon wave vector $\boldsymbol{q}$ and frequency $\omega_\mu(\boldsymbol{q}) = \omega_\mu(0)\bar{\boldsymbol{q}}$ and $\bar{\boldsymbol{q}} = \boldsymbol{q}a$ with $\omega_\mu(0) = v_\mu/a$. Here, v_μ is the sound velocity of phonon branches that takes 1.95×10^4 (1.22×10^4) m/s for LA (TA) [42]. Therefore, the electron–phonon interaction Hamiltonian given by Eq. (5) can be rewritten in the following form:

$$\mathcal{H}_{\mathrm{e-p}} = -\sum_\mu \sum_{\boldsymbol{q}} [\widetilde{M}_\mu b_{\boldsymbol{q},\mu} e^{i\boldsymbol{q}\cdot\boldsymbol{r}} + \mathrm{h.\,c.}]. \tag{7}$$

We have defined $\widetilde{M}_\mu$ as $M_0 M_\mu$ such that

$$M_\mu = \mathbf{1} \otimes \frac{1}{\sqrt{N}}\begin{pmatrix} 0 & M_{AB}(\bar{q}_x + i\bar{q}_y)e^{i\phi(\boldsymbol{q})} \\ M_{BA}(\bar{q}_x - i\bar{q}_y)e^{i\phi(\boldsymbol{q})} & 0 \end{pmatrix}$$

together with $M_0 = \sum_\mu \kappa a_\mu(\boldsymbol{q}) q_0 J_0/2\sqrt{3}$, where $M_{AB} = 1(-i)$ and $M_{BA} = 1(i)$ for LA(TA) branch. Here, $a_\mu(\boldsymbol{q}) = \left(\hbar/2M_C\omega_\mu(\boldsymbol{q})\right)^{1/2}$, and $q_0 = \left(\partial J_0/\partial a\right)/J_0$ is predicted [43,44] around 2.0–2.5 Å^{-1} and κ is the order of ~1/3 for Valance-Force Field method [41,45].

To diagonalize Eq. (1) we regard a unitary transformation technique within the LLP theory [40]. This consists of two successive transformations, the first one eliminates the electron coordinates from Eq. (1), and the second one shifts phonon coordinates by an amount of the interaction strength. To manage this procedure we follow the method that was developed for the investigation of the interaction of electron (hole) with doubly degenerate optical phonon modes of E_{2g} symmetry near the zone center [25,26] and interaction of electron (hole) with phonon mode of A_{1g} symmetry near the zone boundaries [46]. We consider a similar ansatz for the ground-state of the whole system:

$$|\boldsymbol{\Phi}\rangle = \sum_{t'}\sum_{s'} \alpha^{t's'}_{\pm} |t's'\boldsymbol{k}\rangle \otimes U_1U_2|\boldsymbol{0}\rangle_{\mathrm{ph}} \tag{8}$$

such that $\mathcal{H}|\boldsymbol{\Phi}\rangle = E^{ts}|\boldsymbol{\Phi}\rangle$. Here, $|\boldsymbol{0}\rangle_{\mathrm{ph}}$ stands for the phonon vacuum, and $\alpha_{t's'}|t's'\boldsymbol{k}\rangle$ corresponds to electronic state vector defined through the appropriate fractional amplitudes, $\alpha_{t's'}$.

On the one hand, the first unitary transformation

$$U_1 = \exp\left[-i\boldsymbol{r}\cdot\sum_{\boldsymbol{q}} \boldsymbol{q} b^\dagger_{\mu,\boldsymbol{q}} b_{\mu,\boldsymbol{q}}\right] \tag{9}$$

eliminates electron coordinates from Eq. (1), since the transformed operators are given by the relations, $\tilde{b}_{\mu,\boldsymbol{q}} = b_{\boldsymbol{q},\mu}\exp\left[-i\boldsymbol{q}\cdot\boldsymbol{r}\right]$ and $\tilde{\boldsymbol{p}} = \boldsymbol{p} - \sum_{\boldsymbol{q},\mu}\hbar\boldsymbol{q} b^\dagger_{\boldsymbol{q},\mu} b_{\boldsymbol{q},\mu}$. On the other hand, second unitary transformation

$$U_2 = \exp\left[\sum_{\boldsymbol{q}} \widetilde{M}_0\langle t's'\boldsymbol{k}|M^\dagger_\mu|ts\boldsymbol{k}\rangle b^\dagger_{\boldsymbol{q},\mu} - \mathrm{h.\,c.}\right] \tag{10}$$

is the well-known displaced oscillator transformation which shifts phonon coordinates by an amount of the interaction amplitude, $\widetilde{M}_0 = \sum_\mu M_0/\hbar\omega_\mu(\boldsymbol{q})$. It just shifts the phonon coordinates, since it generates the coherent states for the phonon subsystem such that

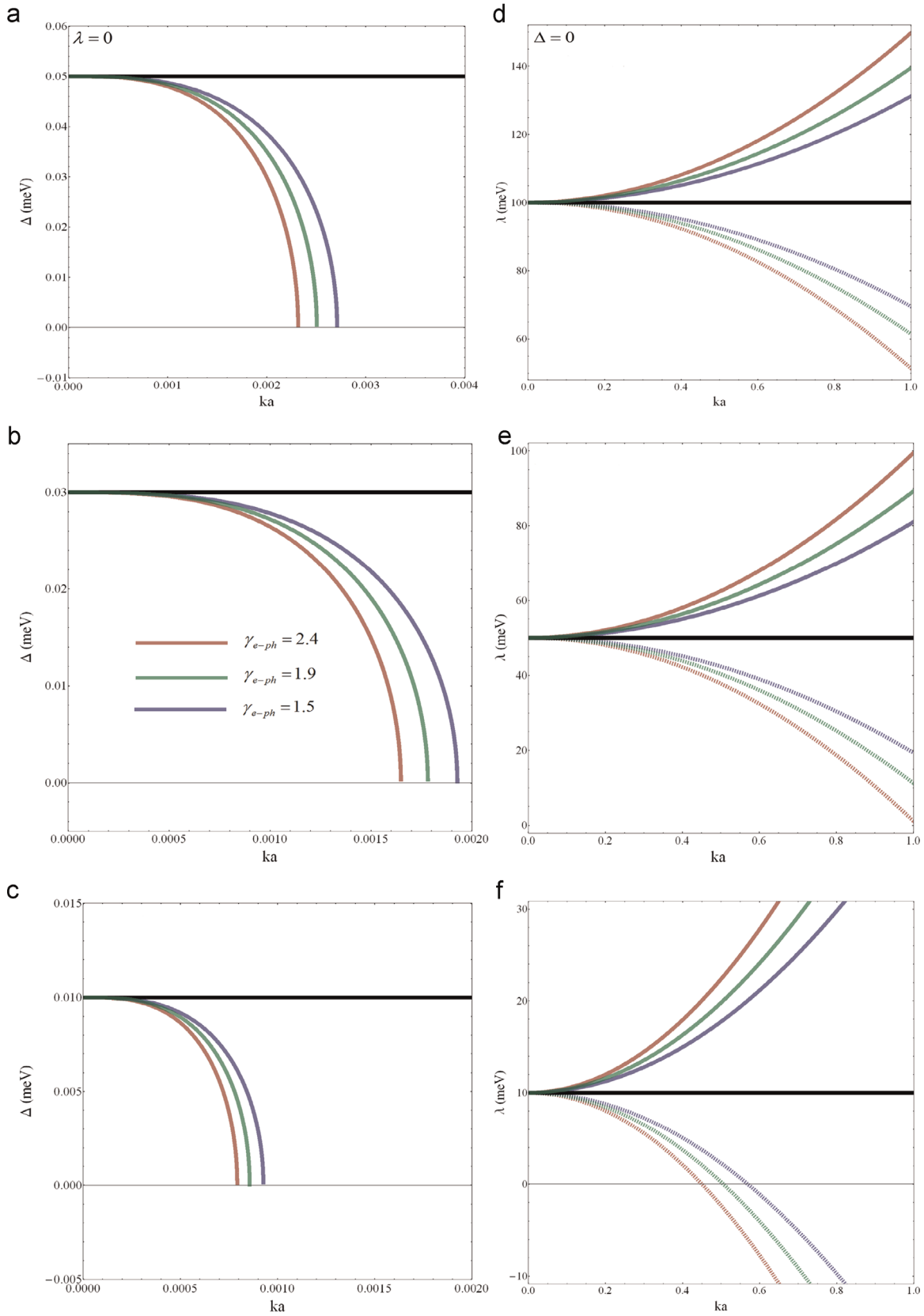

Fig. 1. Effects of electron–phonon interaction on spin–orbit couplings as a function of $\bar{k}_0 = ka$ for different $\gamma_{e-ph} = 1.5$ (blue), 1.9 (green) and 2.4 (red): (a) $\Delta = 0.05$ meV, (b) $\Delta = 0.03$ meV, and (c) $\Delta = 0.01$ meV; (d) $\lambda = 100$ meV, (e) $\lambda = 50$, (f) $\lambda = 10$ for spin-up (dashed) and spin-down (solid) states. (For interpretation of the references to color in this figure caption, the reader is referred to the web version of this paper.)

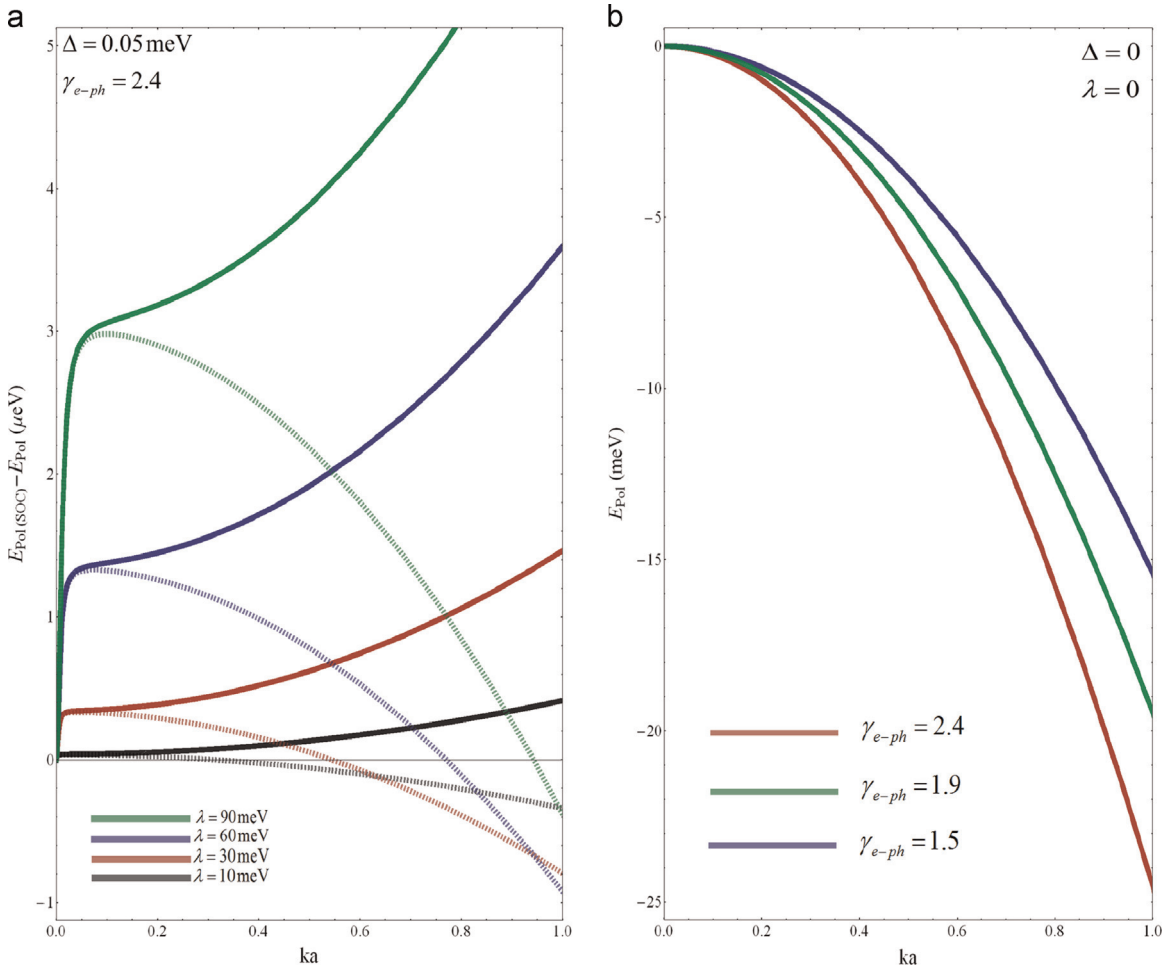

Fig. 2. (a) Difference of polaron self energies at Δ=0.05 meV for different λ=90 meV (green), λ=60 meV (blue), λ=30 meV (red), and λ=10 meV (black), spin-up (spin-down) states corresponds to dashed (solid) lines. (b) Polaron self-energy in the absence of spin–orbit couplings for different γ_{e-ph} = 1.5 (blue), γ_{e-ph} = 1.9 (green), and γ_{e-ph} = 2.4 (red). (For interpretation of the references to color in this figure caption, the reader is referred to the web version of this paper.)

acoustical phonon operators transform according to the rule $\tilde{b}_{\boldsymbol{q},\mu} = b_{\boldsymbol{q},\mu} + \widetilde{M}_0\langle t's'\boldsymbol{k}|M_\mu^\dagger|ts\boldsymbol{k}\rangle$. As a result, under two successive transformation with phonon vacuum, eigenvalues of Eq. (1) can be written as

$$\sum_{t's'} E^{t's'}\alpha_{t's'} = \sum_{t',s',t,s} \Gamma_{ts}^{(1)t's'}\alpha_{t's'} - \sum_{t',s',t,s} \Theta_{ts}^{t's'}\alpha_{t's'} + \delta_{t't}\delta_{s's} - 2\sum_{t',s',t,s} \Gamma_{ts}^{(2)t's'}\alpha_{t's'} + \sum_{t',s',t,s} \Gamma_{ts}^{(3)t's'}\alpha_{t's'} \tag{11}$$

with

$$\begin{aligned}
\Gamma_{ts}^{(1)t's'} &= \hbar v_F\langle s't'\boldsymbol{k}|\mathbf{1}\otimes\boldsymbol{\sigma}\cdot\boldsymbol{p}|s't'\boldsymbol{k}\rangle \\
\Theta_{ts}^{t's'} &= \hbar v_F\sum_{\boldsymbol{q},\mu}|M_0|^2\langle s't'\boldsymbol{k}|\mathbf{1}\otimes\boldsymbol{\sigma}\cdot\boldsymbol{q}|s't'\boldsymbol{k}\rangle|\langle s't'\boldsymbol{k}|M_\mu|s't'\boldsymbol{k}\rangle|^2 \\
\Gamma_{ts}^{(2)t's'} &= \sum_{\boldsymbol{q},\mu}\frac{|M_0|^2}{\hbar\omega_\mu(\boldsymbol{q})}|\langle s't'\boldsymbol{k}|M_\mu|s't'\boldsymbol{k}\rangle|^2 \\
\Gamma_{ts}^{(3)t's'} &= \frac{\lambda}{2}\langle s't'\boldsymbol{k}|(s_y\otimes\sigma_x - s_x\otimes\sigma_y)|s't'\boldsymbol{k}\rangle + \Delta\langle s't'\boldsymbol{k}|(s_z\otimes\sigma_z)|s't'\boldsymbol{k}\rangle
\end{aligned} \tag{12}$$

After taking inner products and converting the sums in Eq. (12) into integrals over $\boldsymbol{q}$, i.e., $\sum_{\boldsymbol{q}} \to \left(S/4\pi^2\right)\int d^2\boldsymbol{q}$, where $S = NS_0$ is the area of the system, and the area of the unit cell is $S_0 = 3\sqrt{3}a^2/2$, it is easy to see that, $\Theta_{ts}^{t's'}$ term vanishes. While performing the q integrals, we consider a cut-off $q \in [0, 2k]$ to avoid divergences. Finally, we arrive at four simultaneous equations for α_{++}, α_{-+}, α_{+-} and α_{--} with considering the summation over s, t, t', and s', which can be rewritten in the following matrix equation:

$$\begin{bmatrix}
\Sigma_{++}^{(1)++} & \Sigma_{-+}^{(2)++} & \Sigma_{+-}^{(3)++} & \Sigma_{--}^{(3)++} \\
\Sigma_{++}^{(2)-+} & \Sigma_{-+}^{(1)-+} & \Sigma_{+-}^{(3)-+} & \Sigma_{--}^{(3)-+} \\
\Sigma_{++}^{(3)+-} & \Sigma_{-+}^{(3)+-} & \Sigma_{+-}^{(1)+-} & \Sigma_{--}^{(2)+-} \\
\Sigma_{++}^{(3)--} & \Sigma_{-+}^{(3)--} & \Sigma_{+-}^{(2)--} & \Sigma_{--}^{(1)--}
\end{bmatrix}\begin{bmatrix}\alpha_{++}\\ \alpha_{-+}\\ \alpha_{+-}\\ \alpha_{--}\end{bmatrix} = 0 \tag{13}$$

with elements

$$\begin{aligned}
\Sigma_{ts}^{(1)t's'} &= \Gamma_{ts}^{(1)t's'} - \Gamma_{ts}^{(2)t's'} + \Gamma_{ts}^{(3)t's'} \\
\Sigma_{ts}^{(2)t's'} &= \Gamma_{ts}^{(1)t's'} - 2\Gamma_{ts}^{(2)t's'} + \Gamma_{ts}^{(3)t's'} \\
\Sigma_{ts}^{(3)t's'} &= -2\Gamma_{ts}^{(2)t's'} + \Gamma_{ts}^{(3)t's'}
\end{aligned} \tag{14}$$

In Eq. (13), characteristic determinant of the whole system can be performed numerically to reach the eigenvalues (E^{ts}) of the Eq. (11). In the absence of electron–phonon interaction, eigenvalues of system yield Eq. (4). In the presence of electron–phonon interaction without SOC, two-fold degenerate eigenvalues of the system can be solved analytically in the following form:

$$E_{e-ph}^{t} = t\left[\left(\frac{3}{2}\bar{k}J_0\right)^2 + 4\left(\frac{1}{48\pi\sqrt{3}}\gamma_{e-ph}\bar{k}^2\right)^2\right]^{1/2} - \left[\left(\frac{1}{48\pi\sqrt{3}}\gamma_{e-ph}\bar{k}^2\right)^2\right] \tag{15}$$

Here, $\gamma_{e-ph} = \sum_{\mu} a_\mu^2(0)/\hbar\omega_\mu(0)$ is the dimensionless constant, and takes values of 1.5–2.4 (q_0=2.0–2.5 Å^{-1}) that qualifies the strength

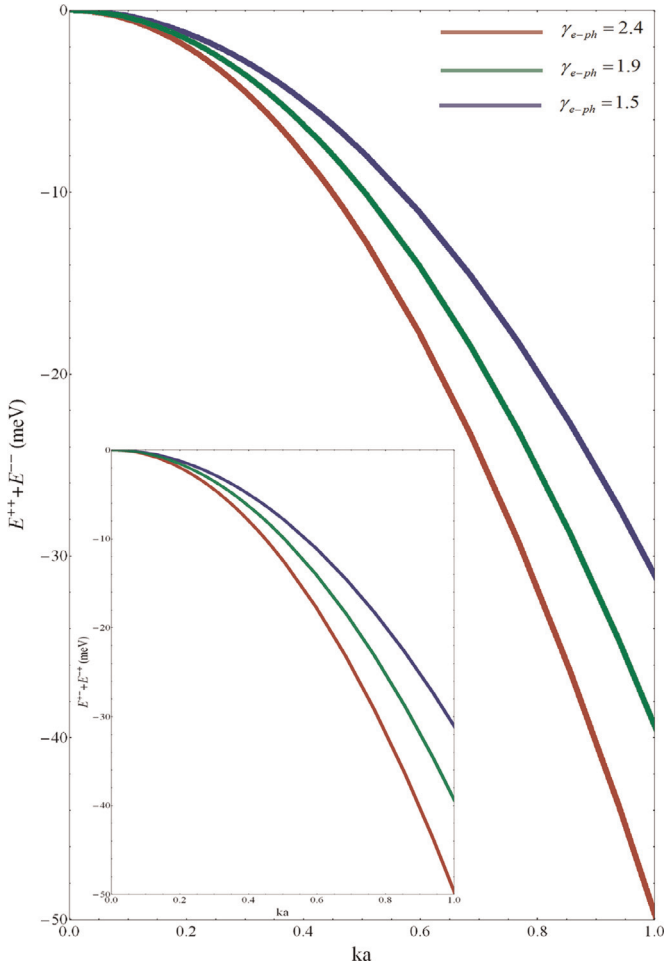

Fig. 3. (Color online) Electron–hole asymmetry due to the electron–phonon coupling, $E^{++}+E^{--}$. Inset: $E^{+-}+E^{-+}$, as a function of $\bar{k}_0$, for $\Delta=0$ and $\lambda=10$ meV.

of electron–phonon coupling. In the absence of electron–phonon interaction, both ISOC and RSOC are constant (black solid lines in Fig. 1). While mass-like term, i.e., Δ only opens gap, and does not lift the spin degeneracy of the system, λ lifts the spin degeneracy, and restores the gapless structure. The status of energy spectrum related with spin–orbit couplings were discussed in Ref. [12] for pristine graphene in detail. In the presence of electron–phonon interaction, we define running spin–orbit coupling constants as a function of $\bar{k}=ka$, γ_{e-ph} for ISOC ($\Delta(\bar{k}, \gamma_{e-ph})$) and $\bar{k}$, γ_{e-ph}, s for RSOC ($\lambda(\bar{k}, \gamma_{e-ph}, s)$). Left panel of the Fig. 1 shows the variation of Δ with respect to $\bar{k}$ and γ_{e-ph} for $\lambda=0$. For small $\bar{k}$'s, Δ become nearly constant, with increasing $\bar{k}$, Δ is decreased and reaches zero at certain critical values of $\bar{k}$. Moreover, with increasing γ_{e-ph}, Δ rapidly vanishes with decreasing $\bar{k}$, and does not take negative value due to the mass-like nature of ISOC term. In other words, energy band gap, creating by ISOC, is closed through the influence of electron–phonon coupling without spin decomposition. In the absence of spin–orbit couplings, second and third terms in Eq. (15) guarantee the gapless band structure. By inclusion of ISOC, energy band gap is generated, damped by the electron–phonon coupling for increasing $\bar{k}$, and rapidly vanished at critical $\bar{k}$ values through the $\sim\gamma_{e-ph}\bar{k}^2$ terms with respect to strength of electron–phonon coupling, γ_{e-ph}. The right panel of Fig. 1 is devoted for RSOC (λ) in the absence of intrinsic spin–orbit coupling. It should be noted that, although we ignore the ISOC term due to its small value, i.e, $\Delta=0.01$–0.05 meV, it can not be removed in realistic situation. It can be easily seen from Fig. 1, while spin-down (solid) states are increased, spin-up (dashed) states are decreased with $\bar{k}$. Spin-up states approach zero values, after compensating the contribution of RSOC, they take negative values beyond the some critical values of $\bar{k}$. Negative values of RSOC are significant for increasing the effects of electron–phonon coupling on the dynamics of charge carriers by the means of bilateral effect, which enhance the polaron formation energy, as it is seen in Fig. 2(a). Possibility of negative RSOC has been extensively discussed in some studies, which can be observed experimentally and foreseen theoretically for ZnO and the other compounds [47–51]. Furthermore, λ is increased (decreased) for spin-down (spin-up) states with increasing values of γ_{e-ph}. It is also obvious that critical values of $\bar{k}$ are shifted to the lower values of ka with decreasing λ (Δ) and increasing γ_{e-ph}.

We also consider the effects of SOC on polaron self-energies of interacting system. Polaron formation, due to the electron–acoustic phonon interaction, is shown in Fig. 2(b). It is easy to see that γ_{e-ph} determines the polaron formation energy, and this energy shifts to lower values with higher γ_{e-ph} couplings. When spin–orbit couplings are switched on ($\Delta=0.05$ meV for different λ), differences between the polaron self-energies together with their effects on spin–orbit couplings ($E^{+s}-E^{+s}_{\mathrm{SOC}}$) and the bare one ($E^{+}_{e-ph}-\hbar v_F k$) are also shown in Fig. 2(a). It is clear that spin–orbit couplings decrease the electron–phonon coupling and also reduce the polaron formation energies. Moreover, due to the RSOC, spin components of these expression show unique character as a function of $\bar{k}_0$. While spin-down states are increased with decreasing $\bar{k}_0$, spin-down states are decreased. Beyond the some critical values of $\bar{k}_0$, they take negative values where the polaron formation energies for spin-up states are enhanced. In other words, while spin-down states decrease the strength of electron–phonon interaction, spin-up states increase it beyond the some critical values of $\bar{k}_0$. Critical values of $\bar{k}_0$ correspond to the condition that spin–orbit couplings have no effects on electron–phonon couplings in pristine graphene. These critical values of $\bar{k}_0$ are also increased with increasing λ, as it is shown in Fig. 2(a). All the analyses are considered for A sublattice ($t=+$), the same procedure can also be performed for B sublattice ($-$). Due to the similar results, it is not presented.

In the absence of electron–phonon coupling, unless the one of the spin–orbit coupling parameters equals zero, there is no electron–hole symmetry in the energy spectrum of the pristine graphene. For $\Delta=0$ and $\lambda\neq 0$, Eq. (4) yields $E^{++}_{\mathrm{SOC}}+E^{--}_{\mathrm{SOC}}=0$ and $E^{+-}_{\mathrm{SOC}}+E^{-+}_{\mathrm{SOC}}=0$ which are the conditions for electron–hole symmetry. By inclusion of electron–phonon coupling, even one of the spin–orbit couplings parameters takes zero ($\Delta=0$, $\lambda\neq 0$ or $\Delta\neq 0$, $\lambda=0$), electron–phonon interaction induces symmetry breaking between electron–hole states. Thus, the conditions indicating the electron–hole symmetry become the function of $\bar{k}_0$ and γ_{e-ph} and deviate from zero. In Fig. 3, the electron–hole asymmetry is presented for different values of γ_{e-ph}. It is clear that asymmetries between electron and hole states are enhanced with increasing $\bar{k}_0$ and γ_{e-ph}. As a result, electron–phonon interaction changes the role of spin–orbit couplings on the energy spectrum of pristine graphene.

3. Conclusion

In conclusion, with the best our knowledge, we present the first theoretical treatment investigating the combined effects of electron–phonon and spin–orbit couplings in pristine graphene. For conventional two-dimensional systems, Covaci and Berciu showed that the polaronic effect is reduced with spin–orbit coupling, spin-up and spin-down states exhibit different conductivities related with this coupling. [37]. We show that variations of polaron formation energy with respect to spin-up and spin-down states exhibit different character. While variations of polaron formation

energy with respect to spin-down states are decreased giving negative contribution to polaron self energy, spin-up states are increased and give rise to an enhancement at polaron self-energy beyond a critical value of $\bar{k}_0$. This results can yield different conductivities for different spin states, as discussed in Ref. [37]. Furthermore, unless one of the spin-orbit coupling parameters takes non-zero value, symmetry between spin-up and spin-down states cannot be constituted [12]. We find that, even only one of the spin–orbit couplings that take zero value, electron–phonon interaction breaks the symmetry between two spin states. We also conclude that, in the effects of electron–phonon interaction, spin–orbit coupling constants become running spin–orbit couplings changing with $\bar{k}_0$ and γ_{e-ph}. While RSOC is either increased or decreased with respect to spin state, ISOC is only decreased as a function of $\bar{k}_0$ without any spin splitting. Our continuum model is valid for only order of $\bar{k}_0 = ka < 1$. For higher values of ka trigonal warp effect should be considered to describe the energy spectrum of graphene. As a result, controlling the spin orientation of charge carriers and their dynamics via spin–orbit and electron–phonon couplings will open the door to projection of graphene-based spintronic nano devices.

Acknowledgements

I thank Professor B.S. Kandemir for valuable discussions. This work is supported by TUBITAK Grant no. 113F103.

References

[1] K.S. Novoselov, A.K. Geim, S. Morozov, D. Jiang, Y. Zhang, S. Dubonos, I. Grigorieva, A. Firsov, Electric field effect in atomically thin carbon films, Science 306 (5696) (2004) 666–669.
[2] K. Novoselov, D. Jiang, F. Schedin, T. Booth, V. Khotkevich, S. Morozov, A. Geim, Two-dimensional atomic crystals, Proc. Natl. Acad. Sci. USA 102 (30) (2005) 10451–10453.
[3] C.L. Kane, E.J. Mele, Quantum spin hall effect in graphene, Phys. Rev. Lett. 95 (22) (2005) 226801.
[4] C.L. Kane, E.J. Mele, Z2 topological order and the quantum spin hall effect, Phys. Rev. Lett. 95 (2005) 146802.
[5] Y. Yao, F. Ye, X.-L. Qi, S.-C. Zhang, Z. Fang, Spin–orbit gap of graphene: first-principles calculations, Phys. Rev. B 75 (2007) 041401.
[6] J.C. Boettger, S.B. Trickey, First-principles calculation of the spin–orbit splitting in graphene, Phys. Rev. B 75 (2007) 121402.
[7] Y.S. Dedkov, M. Fonin, U. Rüdiger, C. Laubschat, Rashba effect in the graphene/Ni(111) system, Phys. Rev. Lett. 100 (10) (2008) 107602.
[8] D. Marchenko, A. Varykhalov, M. Scholz, G. Bihlmayer, E. Rashba, A. Rybkin, A. Shikin, O. Rader, Giant Rashba splitting in graphene due to hybridization with gold, Nat. Commun. 3 (2012) 1232.
[9] S. Datta, B. Das, Electronic analog of the electro-optic modulator, Appl. Phys. Lett. 56 (7) (1990) 665–667.
[10] Y. Semenov, K. Kim, J. Zavada, Spin field effect transistor with a graphene channel, Appl. Phys. Lett. 91 (15) (2007) 153105.
[11] J. Balakrishnan, G.K.W. Koon, M. Jaiswal, A.C. Neto, B. Özyilmaz, Colossal enhancement of spin–orbit coupling in weakly hydrogenated graphene, Nat. Phys. 9 (5) (2013) 284–287.
[12] K. Shakouri, M.R. Masir, A. Jellal, E. Choubabi, F. Peeters, Effect of spin–orbit couplings in graphene with and without potential modulation, Phys. Rev. B 88 (11) (2013) 115408.
[13] T. Stauber, J. Schliemann, Electronic properties of graphene and graphene nanoribbons with 'pseudo-Rashba' spin–orbit coupling, New J. Phys. 11 (11) (2009) 115003.
[14] A. Lopez, Z. Sun, J. Schliemann, Floquet spin states in graphene under ac-driven spin–orbit interaction, Phys. Rev. B 85 (20) (2012) 205428.
[15] H. Min, J. Hill, N.A. Sinitsyn, B. Sahu, L. Kleinman, A.H. MacDonald, Intrinsic and Rashba spin–orbit interactions in graphene sheets, Phys. Rev. B 74 (16) (2006) 165310.
[16] M.O. Hachiya, G. Burkard, J.C. Egues, Nonmonotonic spin relaxation and decoherence in graphene quantum dots with spin–orbit interactions, Phys. Rev. B 89 (2014) 115427.
[17] L. Lenz, D.F. Urban, D. Bercioux, Rashba spin–orbit interaction in graphene armchair nanoribbons, Eur. Phys. J. B 86 (12) (2013) 1–9.
[18] M. Modarresi, B.S. Kandemir, M.R. Roknabadi, N. Shahtahmasebi, Spin dependent transport through triangular graphene quantum dot in the presence of Rashba type spin–orbit coupling, J. Magn. Magn. Mater. 367 (2014) 81–85.
[19] A. Dyrdał, V. Dugaev, J. Barnaś, Spin hall effect in a system of Dirac fermions in the honeycomb lattice with intrinsic and Rashba spin–orbit interaction, Phys. Rev. B 80 (15) (2009) 155444.
[20] S. Abdelouahed, A. Ernst, J. Henk, I. Maznichenko, I. Mertig, Spin-split electronic states in graphene: effects due to lattice deformation, Rashba effect, and adatoms by first principles, Phys. Rev. B 82 (12) (2010) 125424.
[21] M. Gmitra, S. Konschuh, C. Ertler, C. Ambrosch-Draxl, J. Fabian, Band-structure topologies of graphene: spin–orbit coupling effects from first principles, Phys. Rev. B 80 (23) (2009) 235431.
[22] Y. Yao, F. Ye, X.-L. Qi, S.-C. Zhang, Z. Fang, Spin–orbit gap of graphene: first-principles calculations, Phys. Rev. B 75 (4) (2007) 041401.
[23] J. Zhou, Q. Liang, J. Dong, Enhanced spin–orbit coupling in hydrogenated and fluorinated graphene, Carbon 48 (5) (2010) 1405–1409.
[24] S. Konschuh, M. Gmitra, J. Fabian, Tight-binding theory of the spin–orbit coupling in graphene, Phys. Rev. B 82 (24) (2010) 245412.
[25] B.S. Kandemir, Possible formation of chiral polarons in graphene, J. Phys.: Condens. Matter 25 (2) (2013) 025302.
[26] B.S. Kandemir, On the electron-phonon interactions in graphene, Low-Dimensional Functional Materials, Springer, 2013, pp. 77-87.
[27] F.M. Peeters, J.T. Devreese, Acoustical polaron in three dimensions: the ground-state energy and the self-trapping transition, Phys. Rev. B 32 (6) (1985) 3515–3521, http://dx.doi.org/10.1103/PhysRevB.32.3515.
[28] V. Ryzhii, V. Vyurkov, Absolute negative conductivity in two-dimensional electron systems associated with acoustic scattering stimulated by microwave radiation, Phys. Rev. B 68 (16) (2003) 165406, http://dx.doi.org/10.1103/PhysRevB.68.165406.
[29] A. Svizhenko, A. Balandin, S. Bandyopadhyay, M.A. Stroscio, Electron interaction with confined acoustic phonons in quantum wires subjected to a magnetic field, Phys. Rev. B 57 (8) (1998) 4687–4693, http://dx.doi.org/10.1103/PhysRevB.57.4687.
[30] V.I. Pipa, N.Z. Vagidov, V.V. Mitin, M. Stroscio, Electron–acoustic phonon interaction in semiconductor nanostructures: role of deformation variation of electron effective mass, Phys. Rev. B 64 (23) (2001) 235322, http://dx.doi.org/10.1103/PhysRevB.64.235322.
[31] A.L. Magna, R. Pucci, Mobile intersite bipolarons in the discrete Holstein–Hubbard model, Phys. Rev. B 55 (22) (1997) 14886–14891, http://dx.doi.org/10.1103/PhysRevB.55.14886.
[32] E. Cappelluti, Electron–phonon effects on spin–orbit split bands of two-dimensional systems, Phys. Rev. B 76 (8) (2007).
[33] Z. Li, Impact of Dresselhaus versus Rashba spin–orbit coupling on the Holstein polaron, Phys. Rev. B 85 (20) (2012). http://dx.doi.org/10.1103/PhysRevB.85.205112.
[34] C. Grimaldi, Large polaron formation induced by Rashba spin–orbit coupling, Phys. Rev. B 81 (7) (2010).
[35] Z. Li, Z. Ma, A.R. Wright, C. Zhang, Spin–orbit interaction enhanced polaron effect in two-dimensional semiconductors, Appl. Phys. Lett. 90 (11) (2007).
[36] C. Grimaldi, Weak- and strong-coupling limits of the two-dimensional Fröhlich polaron with spin–orbit Rashba interaction, Phys. Rev. B 77 (2) (2008).
[37] L. Covaci, M. Berciu, Polaron formation in the presence of Rashba spin–orbit coupling: implications for spintronics, Phys. Rev. Lett. 102 (18) (2009) 186403.
[38] K. Vardanyan, A. Vartanian, A. Kirakosyan, Two-dimensional Fröhlich polaron with Rashba and Dresselhaus spin–orbit coupling, Eur. Phys. J. B 85 (11) (2012) 1–5.
[39] H. Ochoa, A. Neto, V. Fal'ko, F. Guinea, Spin–orbit coupling assisted by flexural phonons in graphene, arXiv preprint arXiv:1209.4382.
[40] T.D. Lee, F.E. Low, D. Pines, The motion of slow electrons in a polar crystal, Phys. Rev. 90 (2) (1953) 297–302.
[41] H. Suzuura, T. Ando, Phonons and electron–phonon scattering in carbon nanotubes, Phys. Rev. B 65 (23) (2002) 235412.
[42] L. Falkovsky, Phonon dispersion in graphene, J. Exp. Theor. Phys. 105 (2) (2007) 397–403.
[43] L. Pietronero, S. Strässler, H.R. Zeller, M.J. Rice, Electrical conductivity of a graphite layer, Phys. Rev. B 22 (2) (1980) 904.
[44] R.A. Jishi, M.S. Dresselhaus, G. Dresselhaus, Electron–phonon coupling and the electrical conductivity of fullerene nanotubules, Phys. Rev. B 48 (15) (1993) 11385.
[45] W. Harrison, Electronic Structure and the Properties of Solids, WH Freemani and Co., San Francisco, 1980.
[46] B. Kandemir, A. Mogulkoc, Zone-boundary phonon induced mini band gap formation in graphene, Solid State Commun. 177 (2014) 80–83.
[47] S.-H. Wei, A. Zunger, Negative spin–orbit bowing in semiconductor alloys, Phys. Rev. B 39 (9) (1989) 6279.
[48] M. Cardona, G. Harbeke, Optical properties and band structure of wurtzite-type crystals and rutile, Phys. Rev. 137 (5A) (1965) A1467.
[49] J. Fu, M. Wu, Spin–orbit coupling in bulk ZnO and GaN, J. Appl. Phys. 104 (9) (2008) 093712.
[50] K. Shindo, A. Morita, H. Kamimura, Spin–orbit coupling in ionic crystals with zincblende and wurtzite structures, J. Phys. Soc. Jpn. 20 (11) (1965) 2054–2059.
[51] W.R. Lambrecht, A.V. Rodina, S. Limpijumnong, B. Segall, B.K. Meyer, Valence-band ordering and magneto-optic exciton fine structure in ZnO, Phys. Rev. B 65 (7) (2002) 075207.